Università degli Studi di Napoli "Federico II"

SCUOLA POLITECNICA E DELLE SCIENZE DI BASE

DIPARTIMENTO DI INGEGNERIA INDUSTRIALE

CORSO DI LAUREA IN INGEGNERIA AEROSPAZIALE

CLASSE DELLE LAUREE IN INGEGNERIA INDUSTRIALE (L-9)

Elaborato di laurea in Meccanica del Volo

Wind tunnel testing of a wing model with flap and distributed propellers

Relatore:
Prof. Fabrizio Nicolosi

Correlatore:
Prof. Danilo Ciliberti

Candidato:
Alessandra Matera
Matr. N35003184

ANNO ACCADEMICO 2021 – 2022

“A me piacciono le parole forti che vogliono dire qualcosa.”
Louisa May Alcott, Piccole Donne.

Ai miei genitori, il mio porto sicuro.
A Vittorio Grassi, insegnante di vita.

Abstract

The purpose of this work is to present an experimental analysis conducted on a model of a half wing that replicates a wing box structure. These tests were lead in the wind gallery of the Dept. of Industrial Engineering of the University of Naples "Federico II". The main focus is to exploit the new concepts of distributed electric propulsion and its advantages, in order to proceed to the evaluation of aerodynamic coefficients and measurements of pressure distributions and propulsive forces. Data collection and processing was carried out using Excel and a LabView as virtual support tools, which led to the experimental results that will be discussed in the following chapters through charts and tables. Three engine nacelles were analyzed, allowing three different propellers positions; it is interesting to identify which of these is more advantageous in terms of aerodynamic coefficients and section pressure distribution.

Sommario

Lo scopo di questo lavoro è presentare un'analisi sperimentale condotta su un modello di semiala che replica una struttura scatolare alare. Tali prove sono state condotte nella galleria del vento del Dipartimento di Ingegneria Industriale dell'Università degli Studi di Napoli "Federico II". L'obiettivo principale è quello di sfruttare i nuovi concetti di propulsione elettrica distribuita e i suoi vantaggi, per procedere alla valutazione dei coefficienti aerodinamici e alle misure di pressione e forze propulsive. La raccolta e l'elaborazione dei dati è stata effettuata utilizzando Excel e LabView come strumenti di supporto virtuale, che ha consentito di ottenere i risultati sperimentali, i quali verranno discussi ampiamente nei capitoli successivi attraverso l’uso grafici e tabelle. Sono state analizzate tre gondole motore, per tre diverse posizioni delle eliche; è interessante individuare quale tra queste sia più vantaggiosa in termini di coefficienti aerodinamici e della distribuzione di pressione.

Table of contents

List of figures

List of tables

1. Introduction

This chapter aims to introduce the reader to the context in which this thesis was developed, paying particular attention to the motivations and objectives to be achieved.

The wind tunnel experimentations which will be presented in the following chapters were carried out in the Dept. of Industrial Engineering of the University of Naples "Federico II".

1.1 Objectives

The objective of this work is to generate a database of loads, pressure, aerodynamics forces and moments that is significant for a realistic aeronautical design problem. At this aim, a wind tunnel model of a half-wing and instrumented with pressure taps has been investigated.

The tests were performed on three nacelles, at different angles of attack for flaps deflected by 15° and 30°, with and without propellers. The data obtained from the tests provide:

- Evaluation of aerodynamic forces and coefficients;
- Pressure measurements;
- Measurements of propulsive forces.

Subsequently, they were processed in Excel.
The objective of the numerical analyses is to estimate the aero-propulsive effects due to the innovative concept of distributed propulsion on the wing model in the wind tunnel flow regime (low Mach and low Reynolds numbers).

Chapter 2 describes the concepts underlying distributed electric propulsion, analyzing its advantages, disadvantages and the consequent need to validate the numerical analyzes carried out. **Chapter 3** describes the setup of the experimental tests in the wind tunnel: its characteristics, the measurement systems used and the wing model. **Chapter 4** deals with the measurements of the aerodynamic forces and moments, with an insight on pressure distributions. Conclusions are drawn in **Chapter 5**.

2. Distributed Electric Propulsion Concepts

The emergence of distributed electric propulsion (DEP) concepts for aircraft systems has enabled new capabilities in the overall efficiency, capabilities, and robustness of future air vehicles. Distributed electric propulsion systems feature the novel approach of utilizing electrically-driven propulsors which are only connected electrically to energy sources or power-generating devices. As a result, propulsors can be placed, sized, and operated with greater flexibility to leverage the synergistic benefits of aero-propulsive coupling and provide improved performance over more traditional designs.

The rapid growth in flight-weight electrical systems and power architectures has provided new enabling technologies for future DEP concepts, which provide flexible operational capabilities far beyond those of current systems. While a number of integration challenges exist, DEP is a disruptive concept that can lead to unprecedented improvements in future aircraft designs.

NASA has been investigating the benefits of DEP technology, including development of ground test articles, and more recently on the design of a flight demonstrator to establish and verify some of the potential benefits associated with this technology. This flight demonstrator is called Scalable Convergent Electric Propulsion Technology Operations Research (SCEPTOR) project [4].

2.1 Different Implementations of Distributed Electric Propulsion

Distributed Electric Propulsion is not a single integration strategy, but rather a suite of possible airframe-propulsion integrations that can yield net efficiency benefits using different, targeted approaches that may not otherwise be achievable with a few, large propulsion units.

A concept that uses DEP is shown in **Figure 2.1**. It illustrates three types of DEP. The propellers along the leading edge of the wing are used to enhance high-lift performance by increasing the dynamic pressure over the wing at low speeds, enabling a smaller wing. The propellers at the wingtips are used for primary propulsion, and rotate opposite to the wing tip vortex, increasing propulsive efficiency. The single small propeller at the end of the fuselage is used to accelerate the slow moving air along the fuselage boundary layer as a means to “cancel” out fuselage drag. [4]

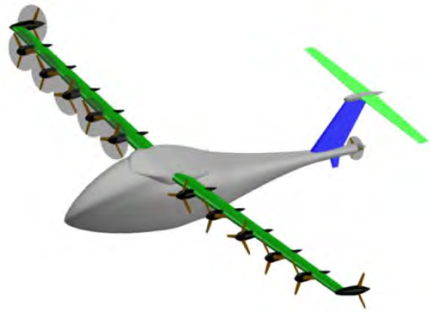

Figure 2.1 – Notional Concept with Three Different Implementations of Distributed Electric Propulsion Technology

One of the major integration benefits of DEP is the use of propellers distributed along the wingspan to enhance the dynamic pressure over the wing at slow speeds. This enables the use of smaller wings for greater high-speed cruise efficiency without compromising low-speed performance, as is necessary for takeoff and landing (particularly out of confined areas).

The high-lift propellers are designed for low-speed operation to enhance dynamic pressure over the wing, rather than for propulsive efficiency at cruise. They are powered down and folded back against their nacelles for low drag at the high-speed cruise point, which is when the flowfield around the wing does not need additional augmentation from the high-lift propellers. Hence, the primary purpose of these propellers is simply to increase the lift of the wing at low speed – they are not designed to provide primary propulsion.

The wingtip-mounted propellers provide primary propulsion. Mounting at the wingtips enables these propellers to be spun against the tip vortex, which results in an increase in propulsive efficiency or a reduction in induced drag, depending on the placement of the props.

2.2 SCEPTOR

“We believed early on that investments needed to be made in electric aircraft propulsion,” says Andrew Gibson, President of ESAero. “We already had a history in this area and had proven that electric aircraft brought benefits; we felt we could meet NASA’s goals for future aircraft.”

This belief led the Central team at ESAero to pursue funding from the NASA Small Business Innovation Research (SBIR) program. After a successful SBIR stint in 2009, ESAero began to focus on non-superconducting technologies, which they felt better aligned with the current supply chain. A few years later, SCEPTOR took form – Scalable Convergent Electric Propulsion Technology Operations Research – which it is allowing NASA to explore the next generation of electric aircraft designs.

2.2.1 Project Goals

SCEPTOR will retrofit an existing aircraft design with DEP technologies, rather than develop a clean-sheet DEP configuration. This enables a significant reduction in demonstration cost and schedule, and also helps to mitigate some risks by associating the systems not modified by DEP with proven designs. The retrofit approach allows for an objective comparison of the aircraft prior to retrofit with the DEP configuration of the same aircraft.

Several incremental demonstrations, dubbed "Mods" (for "modification") are utilized on SCEPTOR to mitigate risk throughout the project, as shown in **Figure 2.2**. The use of an existing vehicle for retrofit, along with the incremental demonstrations, help shape the overall vehicle requirements and "desirements" that are critical to sizing the DEP wing and propulsion systems.

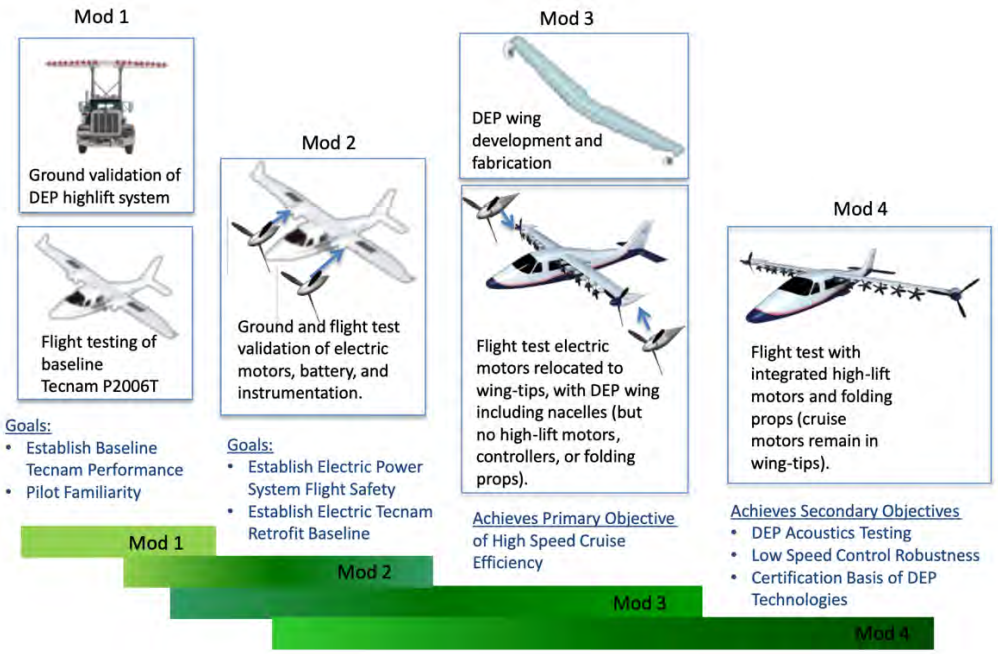

Figure 2.2 – SCEPTOR Incremental Demonstrations ("Mods")

SCEPTOR's primary objective is to demonstrate a large reduction in energy consumption compared to a conventionally-powered aircraft of the same size class in cruise. The "stretch" goal is to demonstrate a fivefold reduction in energy consumption, and the minimum threshold goal is a reduction of a 3.5x.

A typical aviation internal combustion powerplant has an efficiency of approximately 30% when referenced to the lower heating value of the fuel stored onboard the aircraft, whereas modern non-cryogenic electric motors can exceed 90% in combined motor- controller-battery

discharge efficiency. This results in an approximately threefold reduction in energy consumption for the same size and speed class of vehicle. Thus, the lower limit of 3.5x reduction would reflect the full benefit of switching propulsion systems.

Preliminary investigations show that the propulsive-airframe coupling benefits of DEP can exceed multiplier of 1.5 times, enabling an higher wing loading thanks the use of high-lift propellers and the integration of wingtip-mounted cruise propellers. Hence, the project adopted the goal of a total of a fivefold decrease in cruise energy consumption.

2.2.2 Design Approach

The initial configuration for SCEPTOR took the form as introduced by Moore and Fredericks as the first LEAPTech (Leading Edge Asychronous Propeller Technology) concept.

The LEAPTech wing design was used, albeit with a different number of high-lift propulsors, for the SCEPTOR Mod 1 testing of the high-lift propeller concepts on a truck-mounted test platform that was raced along the dry lakebeds at NASA AFRC. The LEAPTech aircraft concept had a high-aspect ratio wing (~18) with a wing loading of approximately 60 pounds per square foot. Its target cruise true airspeed was ~175-200 knots at an altitude of around 10-12,000 feet. This was a deliberately aggressive concept to push technology limits in an attempt to showcase the potential for wing loading increase with DEP. The high aspect ratio was necessary to keep the span loading reasonable – even with the wingtip propellers, a heavily span-loaded wing would have high induced drag at cruise.

The Mod 1 analysis and testing of the LEAPTech wing indicated that aggressive lift augmentation was possible with high-lift propellers. Overall, LEAPTech showed that this lift augmentation factor could exceed twice the maximum lift achievable without the high-lift propellers operating (with flaps alone). This provided the SCEPTOR team with confidence that significant increases in wing loading could occur for the flight demonstration concept. This also helped to shape the design philosophy associated with the SCEPTOR Mod 4 configuration (small wing with both wingtip cruise propellers and leading edge high-lift propellers). Ultimately, the wing would be designed for cruise performance, and for limited performance in the absence of all high-lift propellers (to ensure adequate performance in the Mod 3 configuration). That is, the wing would be sized considering only the performance with the cruise propellers operating, and then the high-lift propellers would be designed to bring the stall speed back to parity with the stall speed of the original (unmodified) aircraft. [4]

3. Wind Tunnel Testing

The wind tunnel is a device involved in experimental aerodynamic research to study the effects of airflow around solid objects. Its use is motivated by a wide interest in practical problems in aerodynamics and by the fact that theoretical and computational methods are not able to provide the full range of results needed to solve many of the above-mentioned problems.

We consider only low-speed wind tunnels, because they make it possible to use models that can be prepared early in design cycles, they include the full complexity of real fluid flow and they can provide large amounts of reliable data. Wind tunnels are often the most rapid, economical and accurate means (with respect to flight test) for conducting aerodynamic research and obtaining aerodynamic data to support design decisions.

There are two basic types of wind tunnels and two basic test-section configurations. However, there are almost endless variations on the specific features of various tunnels. The two basic types are open circuit and closed circuit.

The air flowing through an open circuit tunnel follows an essentially straight path from the entrance through a contraction to the test section, followed by a diffuser, a fan section, and an exhaust of the air. The tunnel may have a test section with no solid boundaries (open jet or Eiffel type) or solid boundaries (closed jet or National Physical Laboratory type). [2]

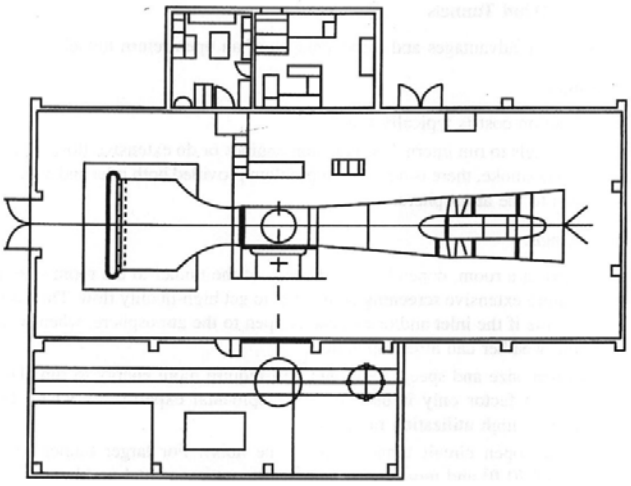

Figure 3.1 – Plan view of an open circuit wind tunnel (Diamler-BenzAerospaceAirbus, Bremen, Germany).

The air flowing in a closed return wind tunnel, Prandtl, or Gottingen type, recirculates continuously with little or no exchange of air with the exterior.

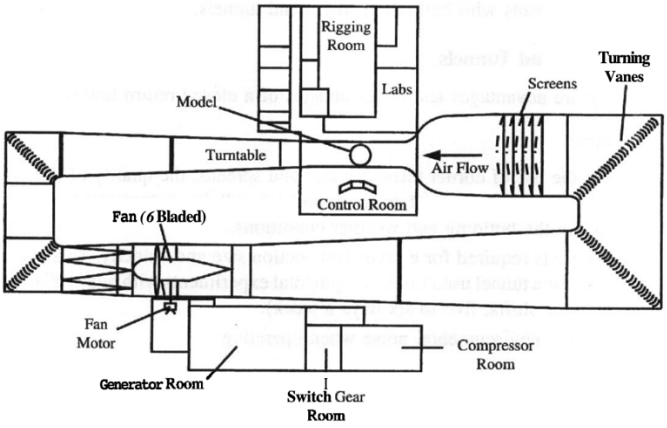

Figure 3.2 – A closed circuit wind tunnel, Defense Establishment Research Agency @ERA), 13 X 9-ft tunnel in Bedford, England.

The great majority of the closed circuit tunnels have a single return, although tunnels with both double and annular returns have been built. Again, the closed circuit tunnel may have either a closed or open test section, and a number have been built that can be run with either an open or closed test section, as needed for a particular experimental program.

3.1 UNINA Low-speed Wind Tunnel Facility

The main subsonic wind tunnel of the Dept. of Industrial Engineering of the University of Naples Federico II is a closed circuit tunnel, closed test section tunnel, which characteristics are summarized in the **Table 3.1**.

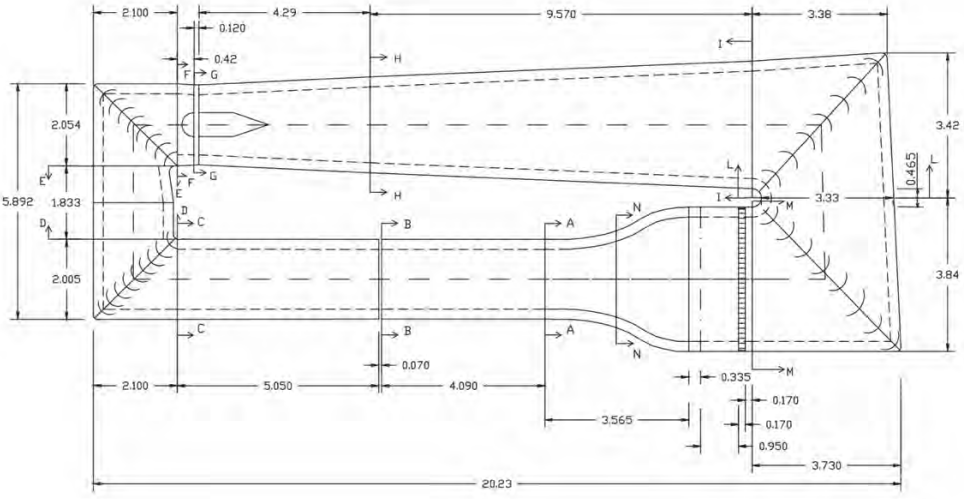

Figure 3.3– Wind Tunnel schematics. Test Section from A-A to B-B

Item	Value
Test section	2.0 m × 1.4 m × 4.0 m (width × height × depth)
Test section frontal area	3.68 m^2
Max power	150 kW
Max flow speed	45 m/s
Turbulence intensity	0.1%

Table 3.1 – Wind Tunnel characteristics

In wind tunnel testing there are some boundaries due by the nature of the tunnel itself. First of all, flow properties may not be the same in space and time. Secondly, the distances of the stream boundaries from the model are less than the corresponding distances for full-scale, in flight operations. Boundaries effects are summarized below. [1]

Downwash – It refers to the component of induced flow in the lift direction at the test model and it is due to the finite distances to the boundaries. In a closed jet, the lift produced is too large and the drag too small at a given geometric angle of attack, corresponding to a smaller downwash.

Upwash – It refers to the component of the flow upstream of the stagnation point diverted upwards, see **Figure 3.4**.

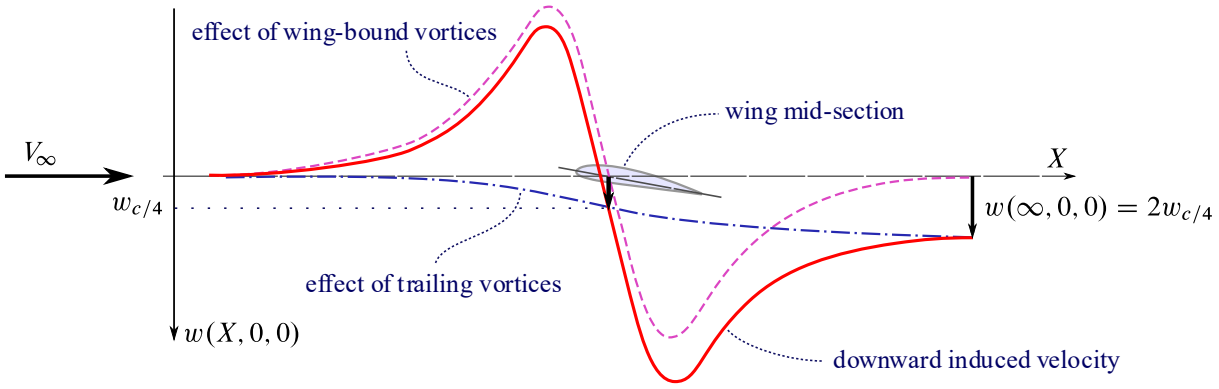

Figure 3.4 – Downwash and Upwash effect

Streamline curvature – It refers to an alteration to the curvature of the streamlines of the flow about a body in a wind tunnel. In a closed tunnel, the lift, pitching moment, hinge moments, and angle of attack are increased.

The correction is proportional to the developed lift and lift coefficient. The correction to be applied is positive, it means that with a certain geometrical angle of attack, the effective corrected angle of attack will be slightly higher.

Solid blockage – It refers to an increase in free-stream velocity around the model caused by the constriction of the flow. It is the most influent effect since it produces a variation in oncoming dynamic pressure.

Wake blockage – When a body is immersed in a moving fluid it produces a wake, whose size is function of the body shape and, in wind tunnel testing, of the ratio between the wake area and the tunnel area, this wake has a mean speed lower than the free stream.

Due to the model solid blockage and the wake blockage, the dynamic pressure around the model will be increased by a factor which is around 1.013. That means :

$$\frac{q_{cor}}{q} = 1.013 \quad or \quad \frac{q}{q_{cor}} = 0.987$$

$$CL_{cor} = CL \cdot \left(\frac{q}{q_{cor}}\right) \qquad CD_{cor} = CD \cdot \left(\frac{q}{q_{cor}}\right) \qquad CM_{cor} = CM \cdot \left(\frac{q}{q_{cor}}\right)$$

3.2 Wing Model

The wing model is a half-wing with three distributed (DEP) propellers, a wingtip mounted (TIP) and a slot flap device. Wing characteristics are reported in **Table 3.2**. The model has been installed on the lateral wall of the wind tunnel, which acts a symmetry plane.

The final version of the test article is a wing model with flap and integrated motors with dedicated load cells. A drawing of the wing model in the test section is shown in **Figure 3.5**. This integrated solution has been chosen to constrain the propellers and the wing in the same reference frame and minimize the aerodynamic interference. In fact, there is no need for an external support structure to keep the motors and propellers close to the wing and at the same angle of attack.

The drawback is that a small, but robust engine frame with force sensors had to be designed and installed inside the wing for each motor. The motor frame allows different horizontal and vertical positions to investigate the effect of propeller position on the blown part of the wing (up-down, close-far). All the electronics, power cables and data cables must be confined inside

the wing, increasing the model weight and reducing the free space to route all the cables, including the pressure taps tubes (**Figure 3.6**).

Even more important, such a solution is prone to vibrations, also because of the limited stiffness of the load cells that must measure light forces from 0.1 to 1 kgf per propeller. This limited the max achievable RPM because of structural resonance of the motor assembly. This effect was not anticipated, because a preliminary numerical modal analysis provided a significantly higher range of natural frequencies.

Item	Value
Airfoil	GAW-1 17%
Planform	Rectangular
Wingspan	1.4 m
Aspect ratio AR	7.0 (3.5 half-model)
Chord	0.4 m
Planform area	0.56 m^2
DEP propellers diameter	0.3 m
TIP propeller diameter	0.4 m
Pressure taps lines	3 lines for about 90 taps
Flap chord ratio c_f/c	0.3
Inner flap position	0.2 m
Inner flap position	1.1 m

Table 3.2 – Wing model characteristics

As concern the nacelle, it was decided to design a unique body for all the possible motors positions, so that differences in aerodynamic coefficients are due to aero-propulsive effects only and not to nacelle shape. For this reason, the nacelle appears bigger than usual, enveloping all the possible engine configurations. Only the nacelle nose changes to accommodate the various propeller positions, both horizontally and vertically.

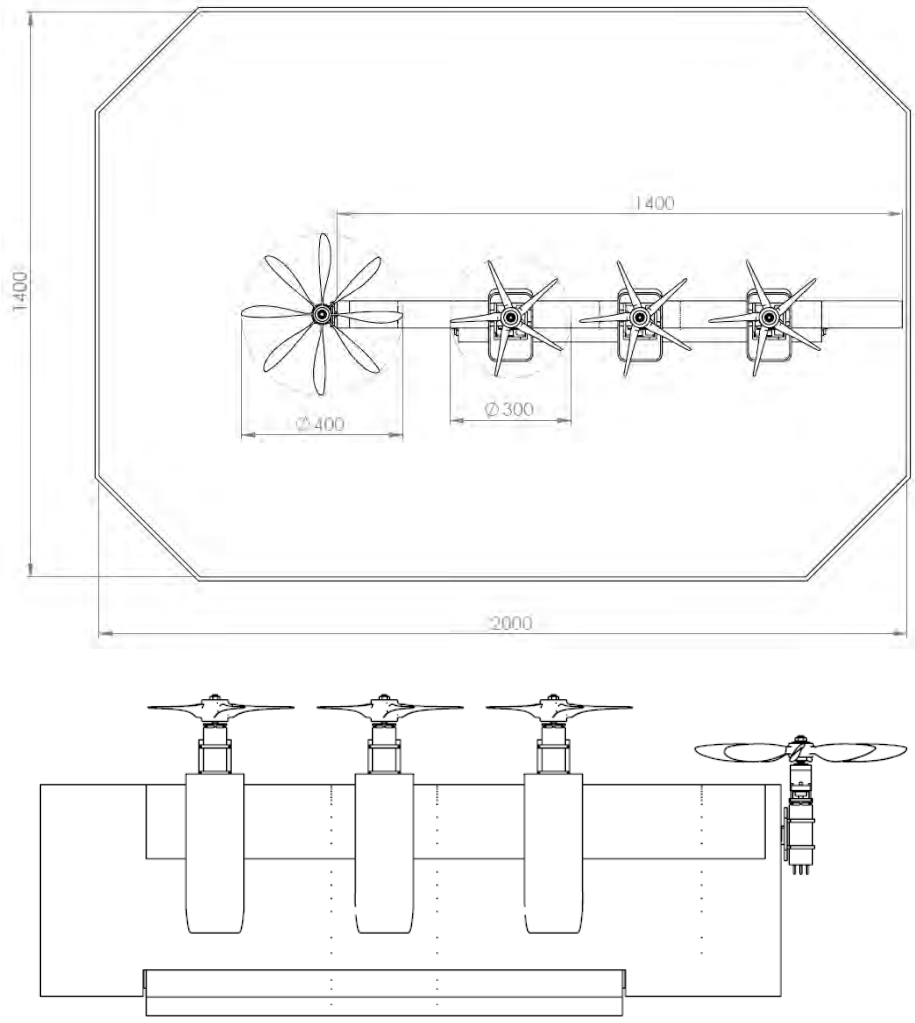

Figure 3.5 – Drawings of the wing model installed in the wind

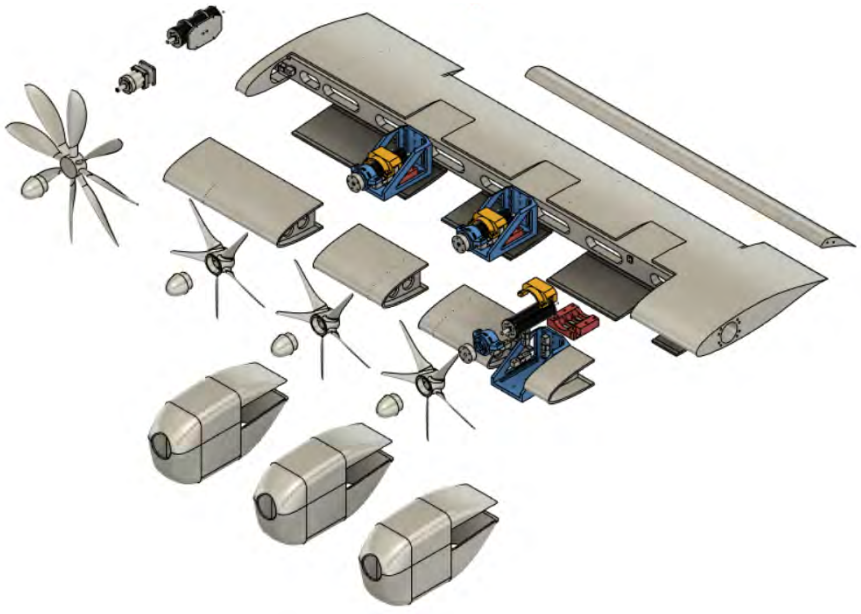

Figure 3.6 – Wing model assembly

3.3 Distributed Propeller Design

Distributed propellers have the main objective of increase the wing lift coefficient per given angle of attack and flight speed. Of course, thrust will be produced at the same time, but such a propeller is not optimized to provide thrust.

The best way to increase the lift capability of a wing with a propeller is to uniformly blow on the lifting surface. Thus, propeller must not be designed for minimum induced loss (MIL), as usual, but to provide a flow speed higher than flight speed uniformly distributed in a streamtube behind the propeller disk.

It is expected that these propellers operate in take-off, landing, and/or climb conditions. According to the latest scientific reports on distributed electric propulsion, one of the most important parameters is the diameter to chord *D/c* ratio, which should be of unit order of magnitude to achieve significant blowing effects.

To measure a significant aero-propulsive effect, it was decided to design the model such to blow on the wingspan portion covered by the flap which is about 0.9 m. Three high-lift (DEP) propellers have been designed with a diameter of 0.3 m each. The DEP propeller has been designed to work below 5000 RPM to be compatible with the available Lehner 2280 inrunner electric motors without installing a gearbox. [3]

Item	Value
Propeller diameter	0.3 m
Design airspeed	20 m/s
Design RPM	5000
Section design Cl	0.8
Propeller mass	0.15 kg excluded hub spinner and installation support

Table 3.3 – DEP propeller characteristics

3.4 Data Acquisition and Control System

The data acquisition and control system is made up of several electronic components.

- National Instruments NI-6343 device (hardware) for the acquisition and conversion into 16 bit of output data coming from the measurement instrumentation.
- A desktop PC, provided with an interface software for the SmartZoc Pressure Sensors.

- LabView virtual instruments developed at UNINA (software) allow the creation of an interactive language and environment for developing test, measurement and control applications with quick access to hardware and results. This software also facilitates the automation of experiments by allowing you to quickly acquire and view data from any type of instrument.

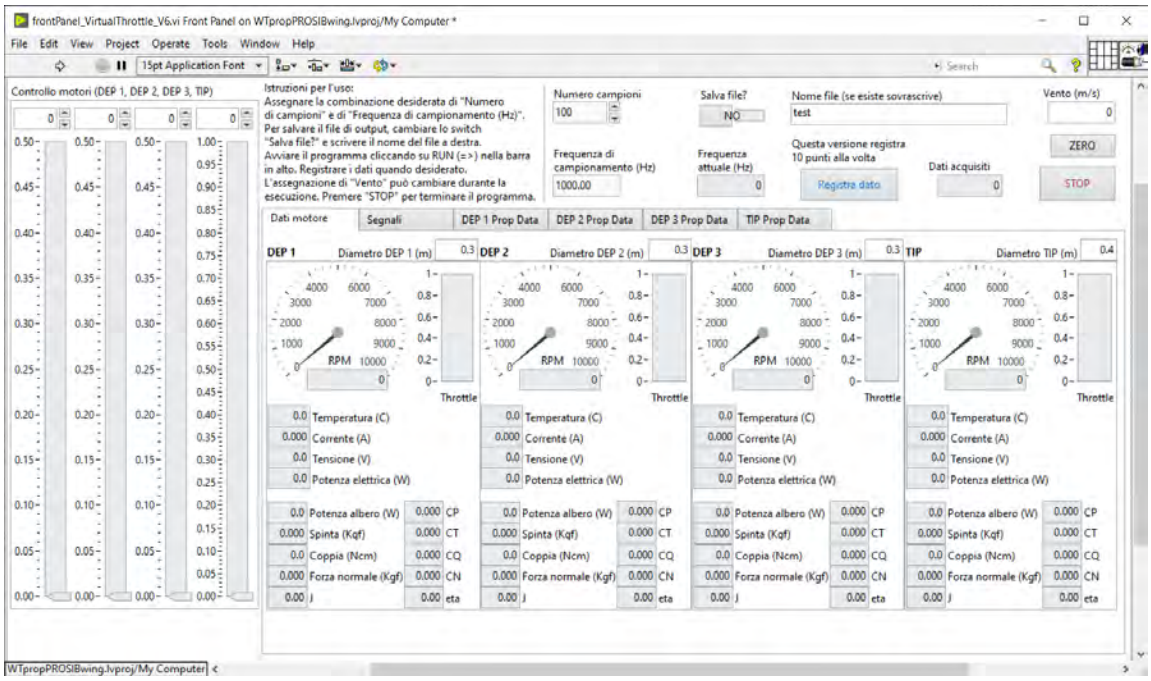

Figure 3.7– LabView VI front panel

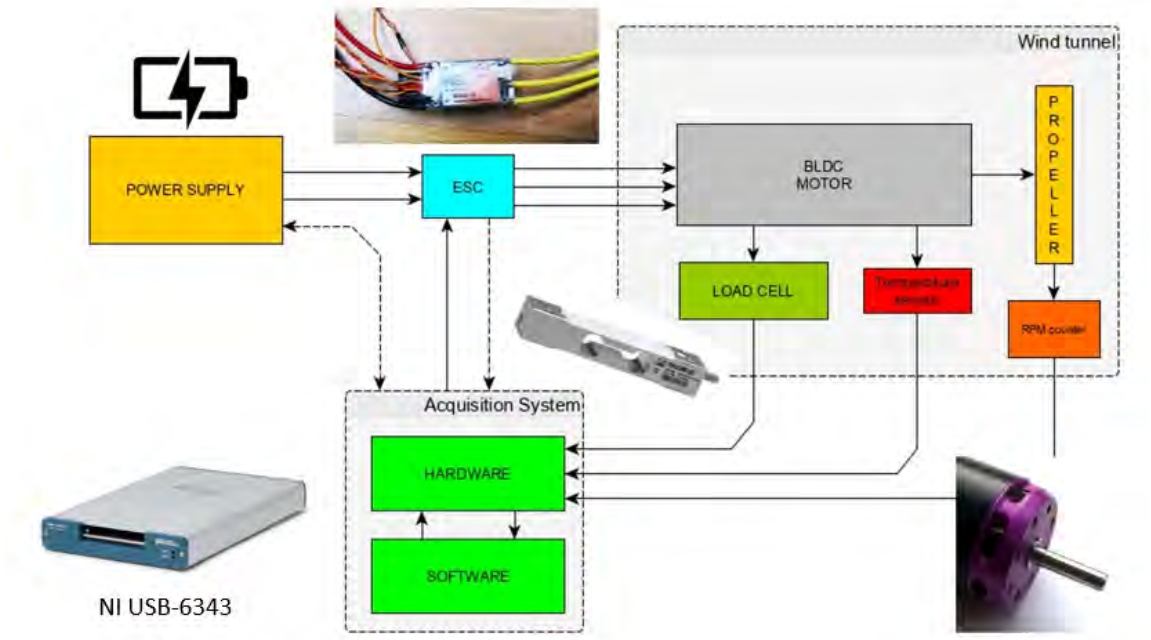

Figure 3.8 – Data acquisition and control system

4. Experimental Results

The wind tunnel tests have been originally planned at a flow speed of 20 m/s to get an acceptable Reynolds number while at the same time not bringing the wind tunnel balance strain gauges over the full scale in the predicted range of achievable aerodynamic forces, accounting for flap and propeller blowing effects.

The measurement ranges and accuracy are described below.

Component	Range		Accuracy
	Min	Max	
Normal force (Lift) L	−80 kgf	100 kgf	0.030 kgf
Horizontal force (Drag) D	−12 kgf	12 kgf	0.005 kgf
Pitching moment M_Y	−15 kgf·m	15 kgf·m	0.010 kgf·m
Bending moment M_{fl}	−40 kgf·m	60 kgf·m	0.030 kgf·m
Yawing moment M_{yaw}	−8 kgf·m	8 kgf·m	0.006 kgf·m

Table 4.1 – Wind tunnel external balance range and accuracy data

The set of experimental data regard the wing with the application on the leading edge of three nacelle with flap deflected. This tests concern about the effects of distributed electric propulsion blowing on the flap at several angles of attack, from zero to ten degrees. Prior to these, preliminary tests were made to prevent the formation of laminar bubbles and forcing the flow transition by means of trip strips. These are not shown here for the sake of brevity.

4.1 Effects of Distributed Propulsion

The effects of DEP are here evaluated. To get a fair comparison between prop-on and prop-off tests, both have been run with the nacelle installed. For the prop-off configuration, the propellers have been removed, leaving only the nacelle with a flat motor hub. In any case, the TIP propeller and its motor assembly has been removed.

Because of structural resonance induced by vibrations above 5000 RPM, the full potential of the test model could not be exploited. For safety reasons, the rotational rate of the propellers has been reduced to a maximum value of 4200 RPM. At the same time, to preserve the propeller design advance ratio and pressure jump, the flow speed has been reduced from 20 m/s to 12 m/s.

The installed propeller characteristics have been measured. The net thrust has been calculated by removing the motor drag fixture. [3]

Photos and charts of the aerodynamic coefficients are reported in the following pages. Configurations with flap deflection at 15° and 30° have been investigated.

Figure 4.1 **–** DEP prop-off configuration

Figure 4.2 **–** DEP prop-on configuration

Figure 4.3 – DEP prop-on configuration: perspective

Figure 4.4 – DEP prop-on in action

In order to evaluate the effects of DEP, it is sufficient to observe the relative increments in the curves of **Figure 4.5** and **4.6**. The charts show the trend of the aerodynamic coefficients (C_L, C_D, C_M) without propellers (prop-off) and with propellers rotating up to 4200 RPM, respectively with 15° and 30° of flap deflection. In the following charts, the reference point for the pitching moment evaluation is set at *c*/4.

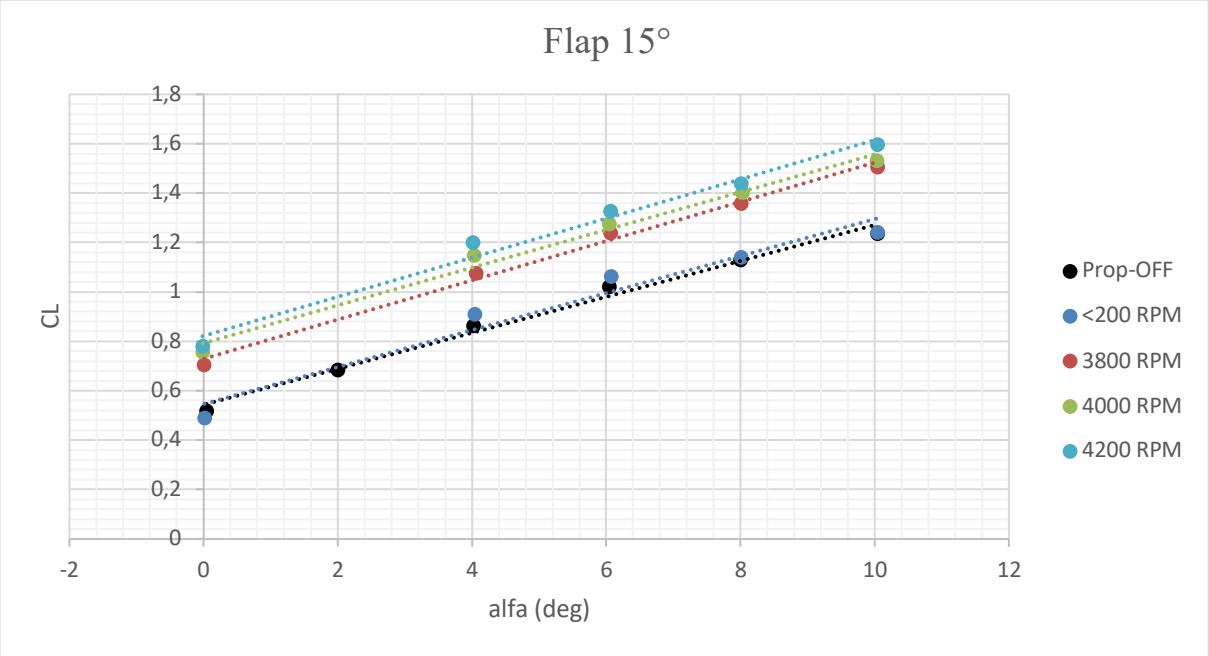

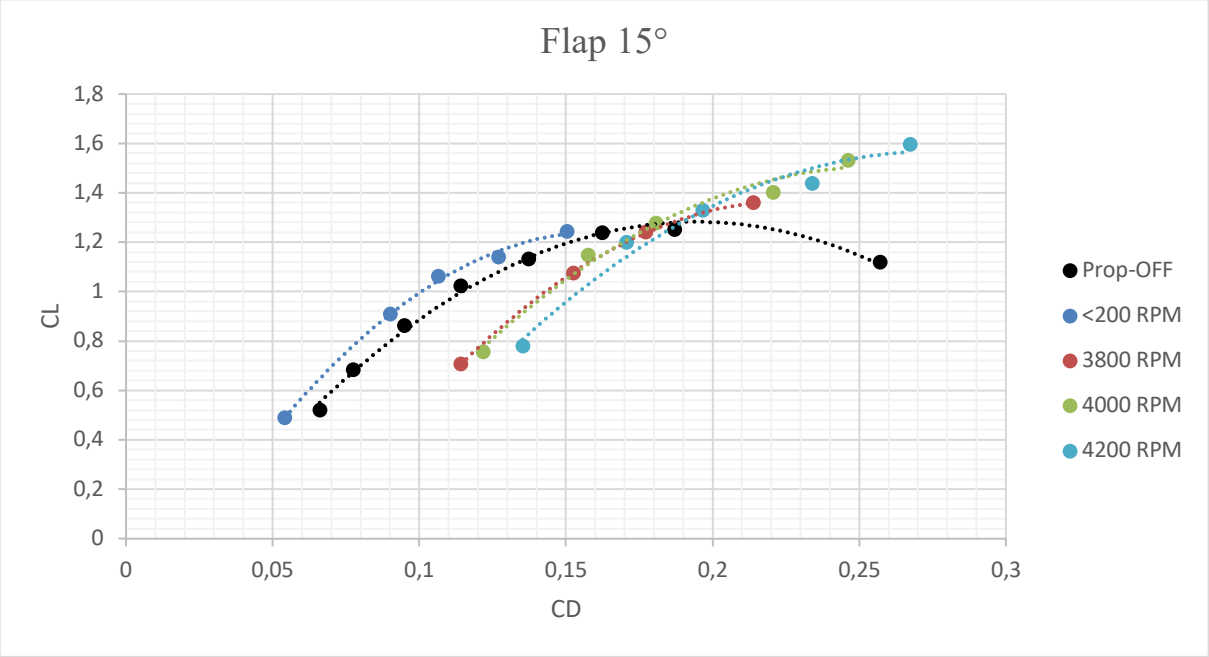

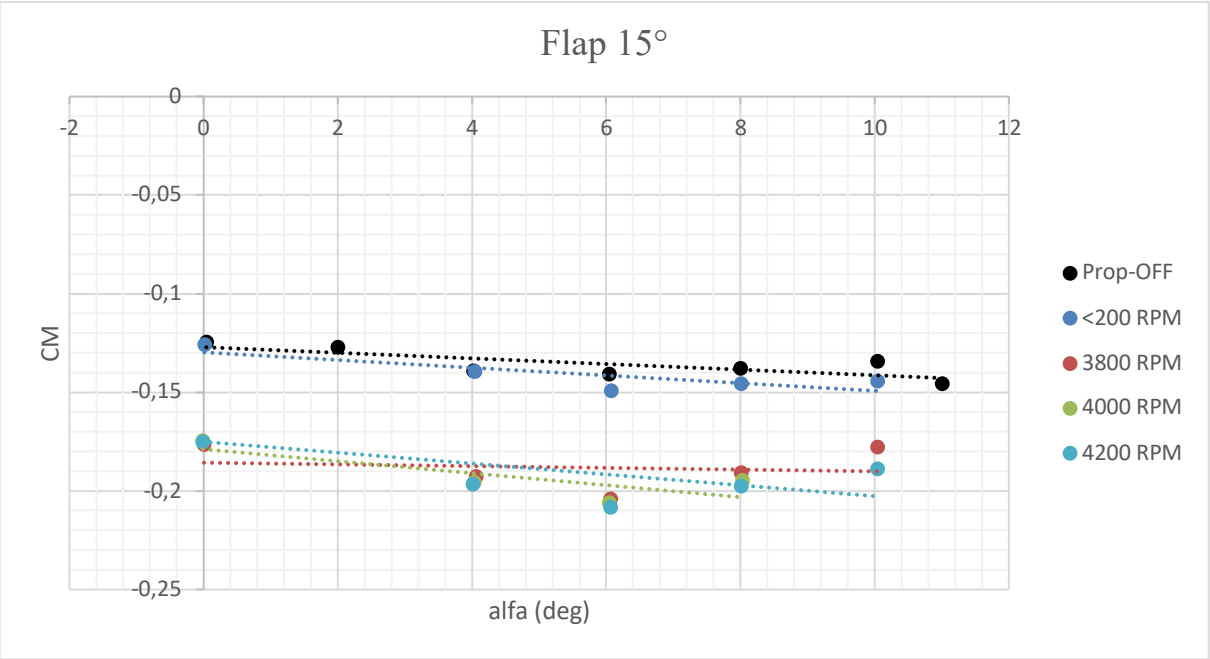

Figure 4.5 – Experimental DEP data, flap 15°, Nacelle 1

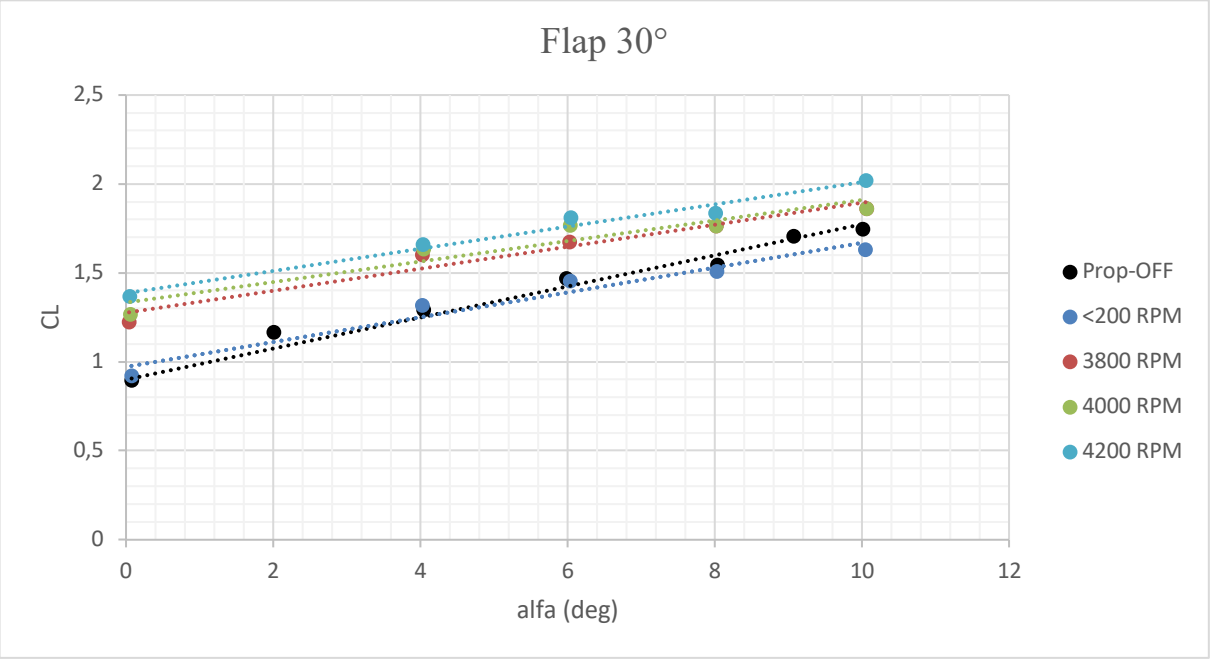

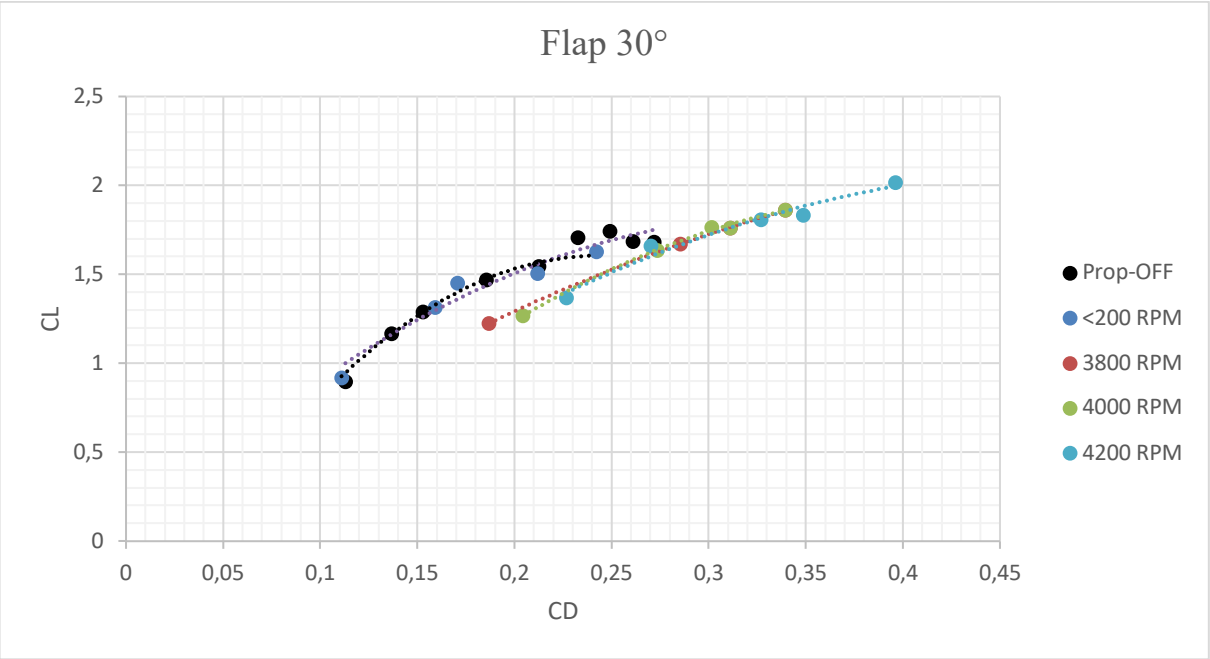

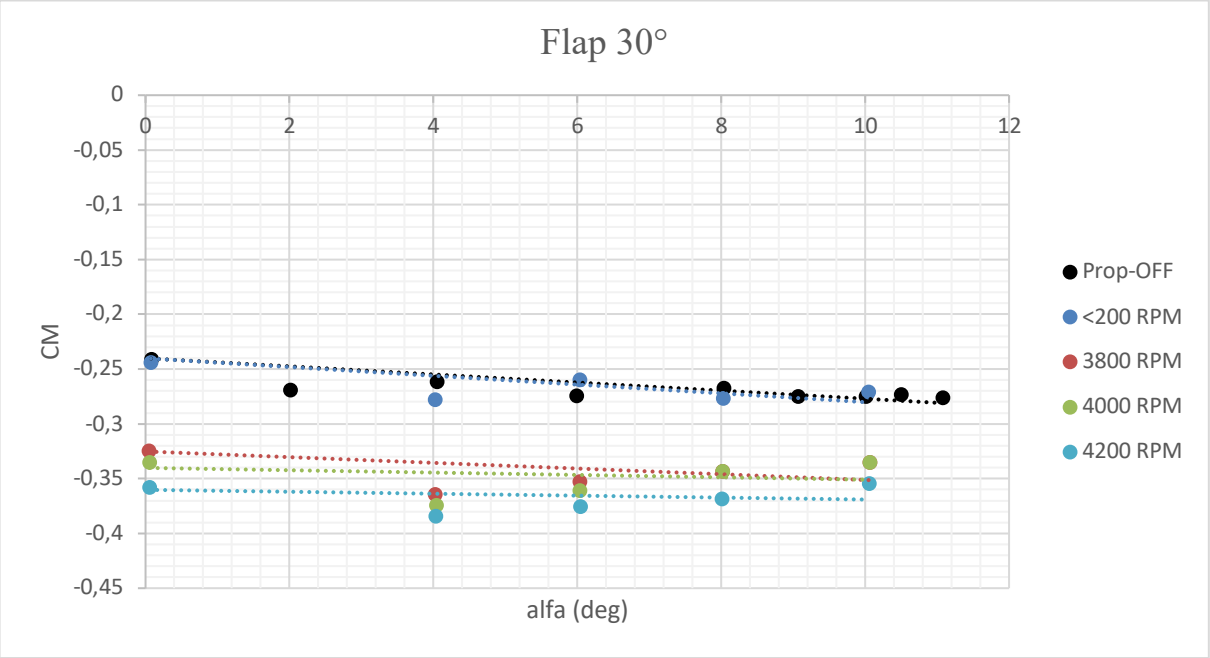

Figure 4.6 – Experimental DEP data, flap 30°, Nacelle 1

To better highlight the difference recorded between the coefficients when the flaps are deflected, the following increments are shown in **Table 4.2**: $\Delta C_L, \Delta C_M, \Delta C_{D0}$, $C_{L\alpha}$ ratio, and $C_{M\alpha}$ ratio, where ΔC_{D0} is the increase of the drag coefficient at zero lift.

The linear part of the lift curve can be mathematically represented by: $C_L = C_{L\alpha}(\alpha - \alpha_0)$.

In which, $C_{L\alpha}$ is the symbol for the so called lift curve-slope, in l/rad – this quantity has a theoretical value of 2π per radian for very thin airfoils – and α_0 is the angle of attack for zero lift and it's typically negative. From this it is possible to evaluate the increase in the $C_{L\alpha}$.

In the same way, $C_{M\alpha}$ is defined as the moment curve-slope. It induces a forward shift towards the leading edge.

	Flap 15°	**Flap 30°**
ΔC_L at $\alpha = 0°$	0.26	0.47
ΔC_L at $\alpha = 10°$	0.36	0.27
$C_{L\alpha,on}/C_{L\alpha,off}$	1.089	0.77
ΔC_{D0}	0.0413	0.0229
ΔC_M at $\alpha = 0°$	−0.051	−0.120
ΔC_M at $\alpha = 10°$	−0.043	−0.079
$C_{M\alpha,on}/C_{M\alpha,off}$	1.143	0.409

Table 4.2 – Increase of the aerodynamics coefficients

In the following charts the section pressure distributions at selected angles of attack will be shown. As illustrated in **Figure 4.7**, Sez.1 refers to a line of pressure taps at 75% radius inboard of the center DEP propeller, Sez.2 refers to the 75% radius outboard, and Sez.3 refers to a pressure taps line in the TIP propeller region (here the tip propeller was not installed).

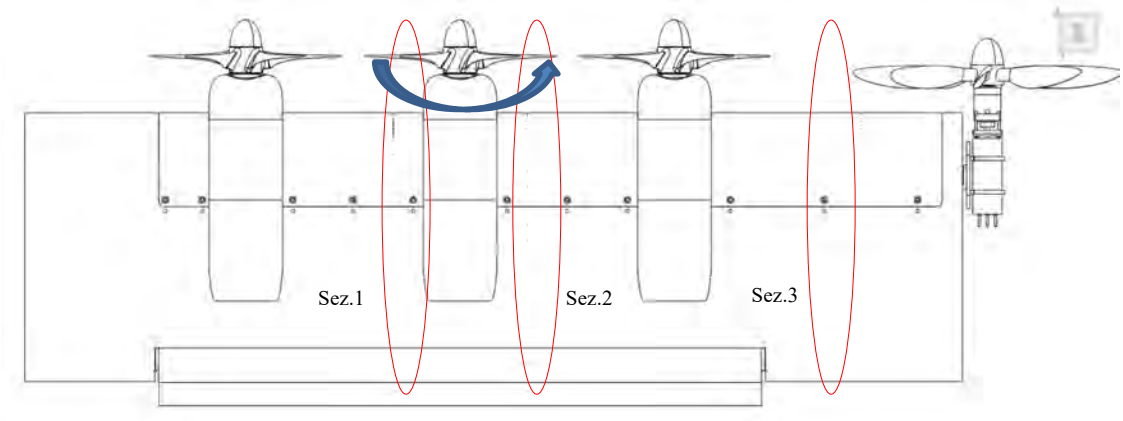

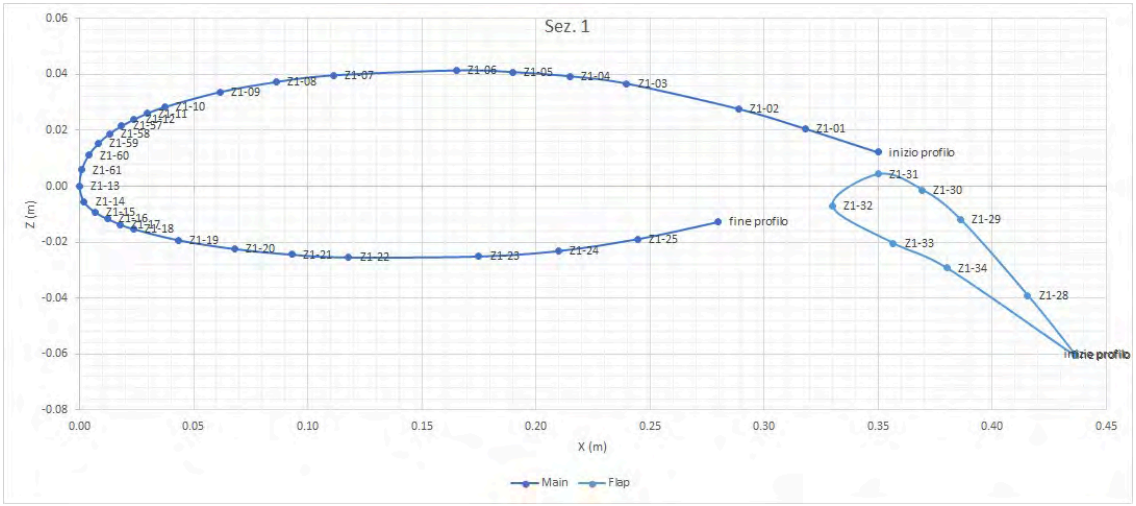

Figure 4.7 **–** Pressure taps lines and section distribution

The effect of propeller blowing is apparent. In the wind tunnel conditions (*Re* = 330000, Ω = 4200 RPM), the inboard section achieves a higher *Cp* peak with respect to the unblown conditions, because of the angle of attack induced by the propeller causing un upwash. Conversely, the outboard section achieves a lower peak with respect to the prop-off conditions (propeller induced downwash).

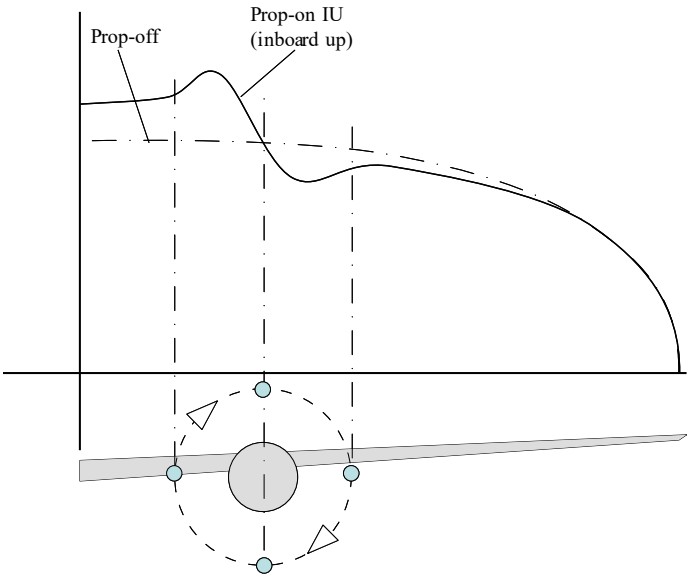

Figure 4.8 **–** Prop wing loading inboard up scheme

As we know, propeller is made up of two or more fluid dynamic elements, called blades. They act as "spinning wings", causing the variation of the momentum in the direction of the forward speed.

In **Sec. 1**, the blade rises and the angle of attack increase. The effects recorded are mainly three: the blowing propeller, the upwash and the flaps deflected. Instead, in **Sec. 2**, it's quite the opposite since the blade goes down and the angle of attack decrease. There's always the blowing propeller and the effects of the flaps, but there won't be upwash but downwash.

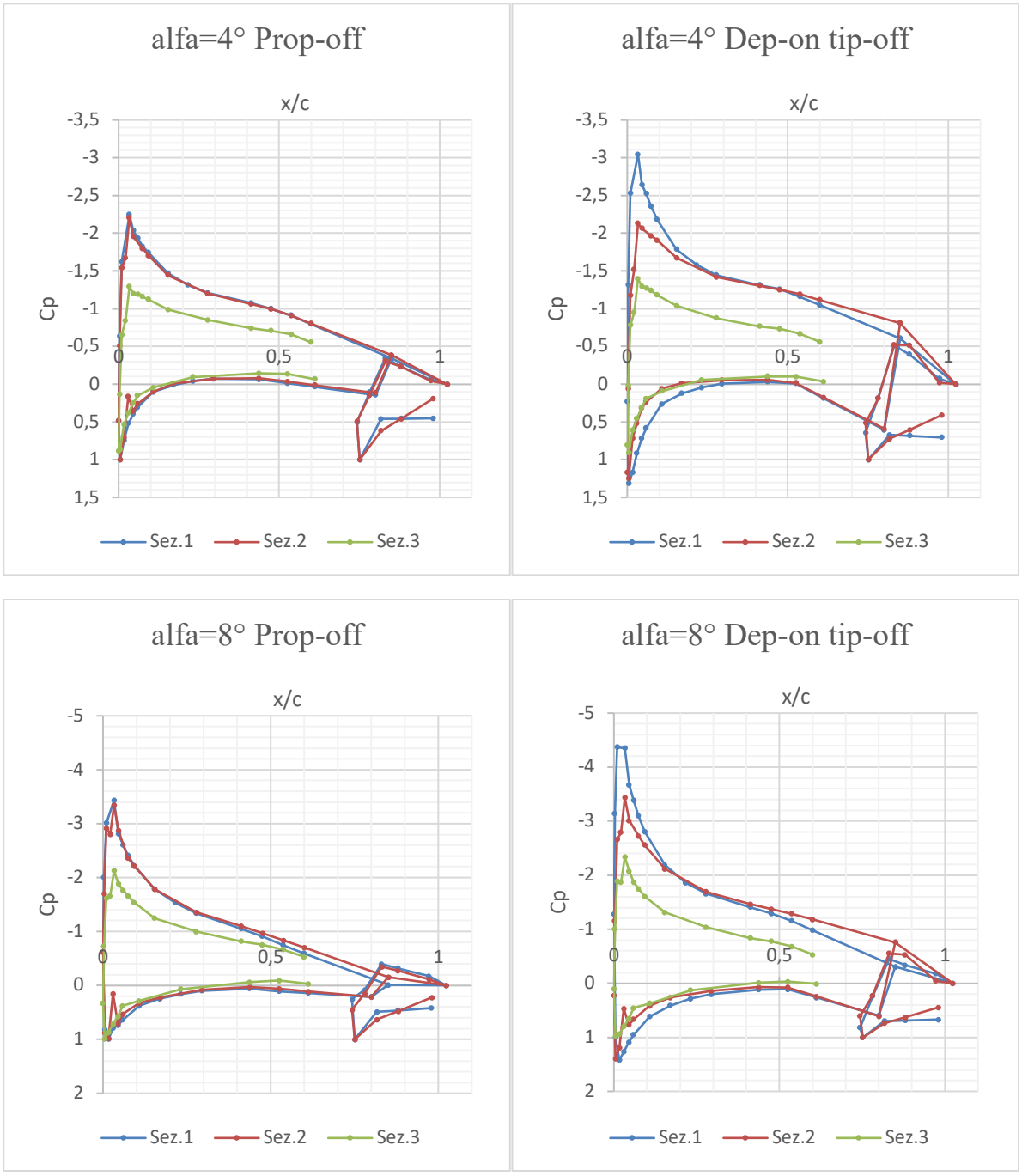

Figure 4.9 – Section Cp distributions, comparison per condition, flap 15°, Nacelle 1

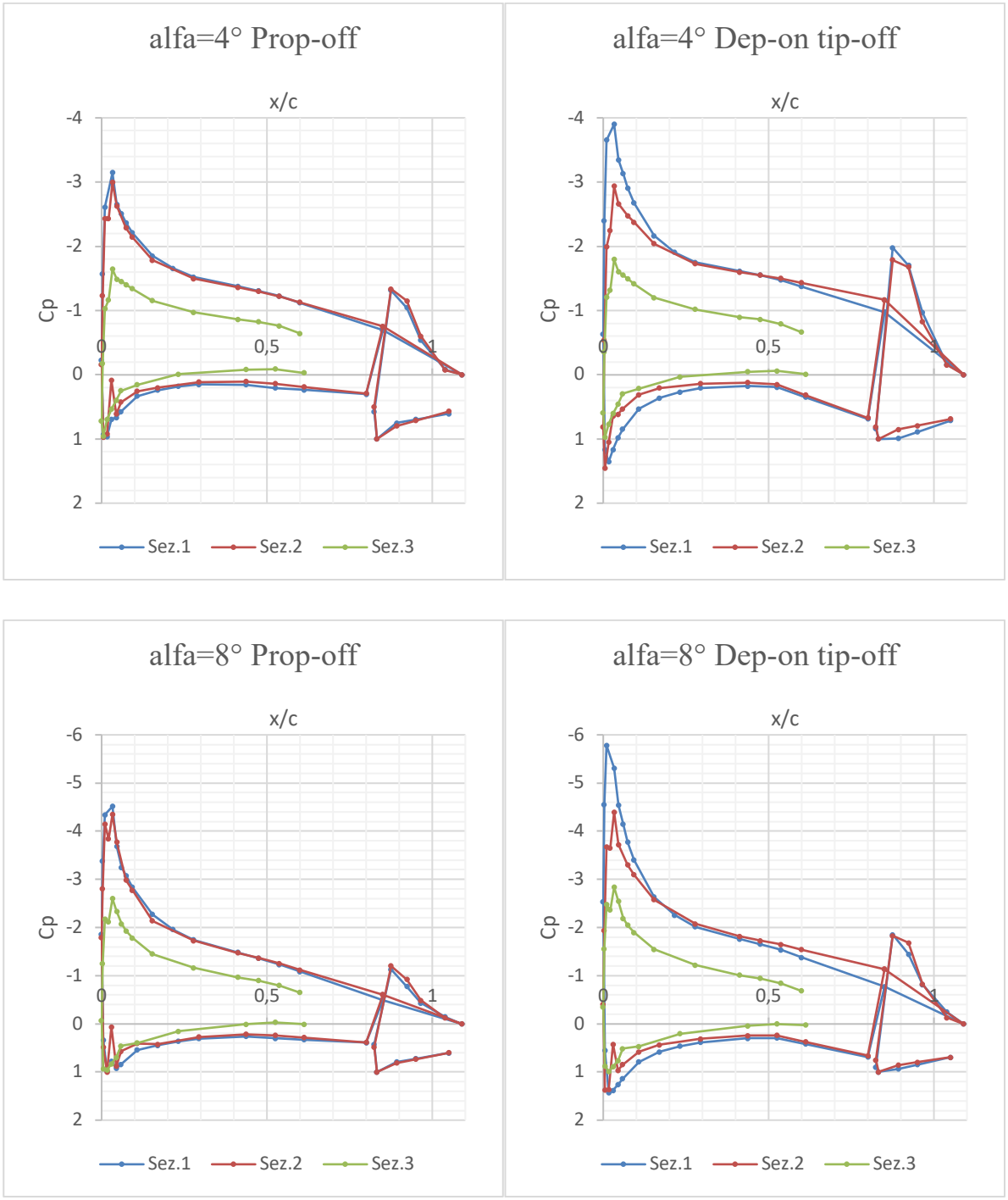

Figure 4.10 – Section *Cp* distributions, comparison per condition, flap 30°, Nacelle 1

It follows the direct comparison between prop-on and prop-off conditions for the two sections around the central DEP propeller. The third section is not considered, since the tip was not installed and there were not carried out experimental tests.

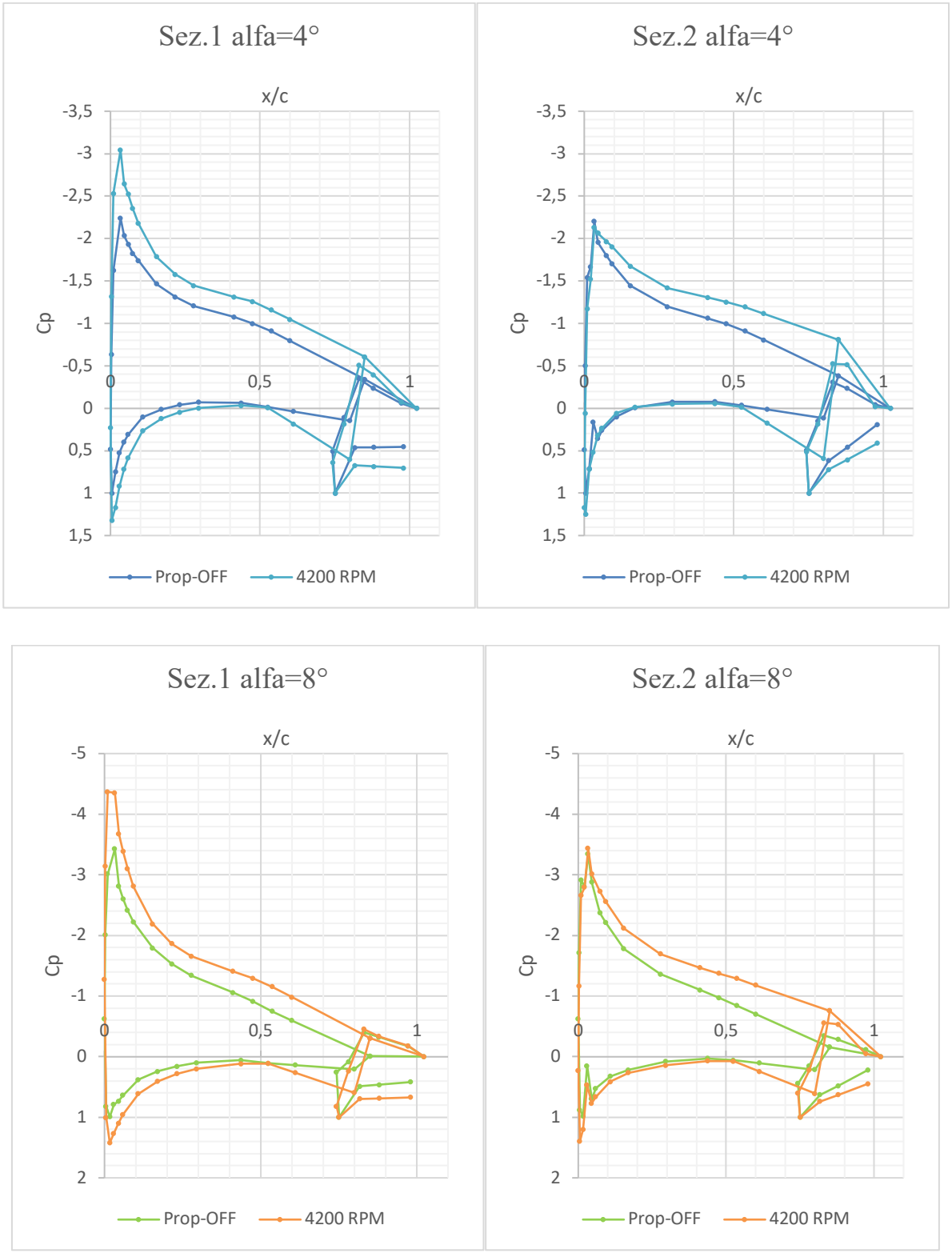

Figure 4.11 – Section *Cp* distributions, comparison per section, flap 15°, Nacelle 1

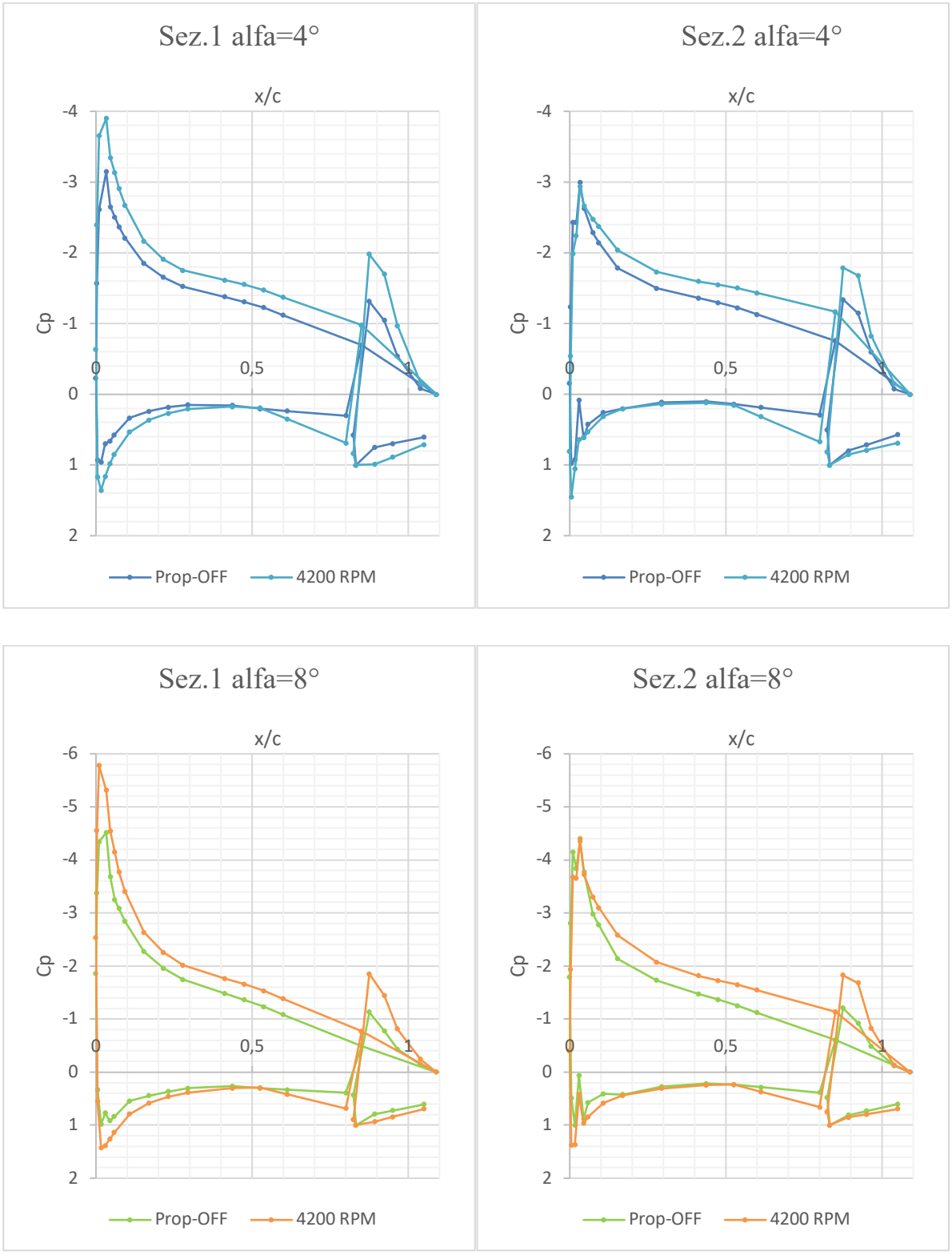

Figure 4.12– Section *Cp* distributions, comparison per section, flap 30°, Nacelle 1

Repeatability is the closeness of the agreement between the results of successive measurements of the same measure, when carried out under the same conditions of measurement. It is sometimes considered useful perform some repeatability tests to confirm the experimental results. A few repeatability tests have been performed and since the results are close to each other, it is reasonable to assume that the tests are reliable. The average errors on the measured aerodynamic coefficients are reported in **Table 4.3** and **Table 4.4** for prop-off and prop-on conditions respectively.

Nominal value	**Average error**			
A	α	C_L	C_D	C_M
0°	n.a.	1.43%	0.94%	−0.44%
2°	1.84%	5.60%	1.20%	−1.55%
4°	0.41%	1.99%	2.80%	−1.88%
6°	0.33%	1.00%	2.44%	−2.49%
8°	0.20%	0.88%	2.69%	−3.81%
10°	0.20%	3.18%	0.15%	−1.65%

Table 4.3 – Repeatability tests in prop-off condition, flap 30°

Nominal value	**Average error**			
A	A	C_L	C_D	C_M
0°	n.a.	5.31%	2.99%	−0.36%
2°	n.a.	n.a.	n.a.	n.a.
4°	0.55%	1.65%	1.65%	−2.01%
6°	0.22%	3.40%	1.41%	−0.70%
8°	0.41%	1.28%	0.37%	−2.06%
10°	0.28%	1.41%	2.04%	−1.18%

Table 4.4 – Repeatability tests in prop-on condition, flap 30°

4.2 Comparison of DEP array positions

In the previous sub-sections, results for a single nacelle have been reported. The propeller rotation axis collinear to the prop wing chord. The experimental tests on the other two nacelle presented quite similar results, hence it was considered unnecessary to report them. Next, the comparison of DEP array position is presented, to identify which of the three is the best option. DEP array can be moved in four positions, but the fourth nacelle was not object of this investigation.

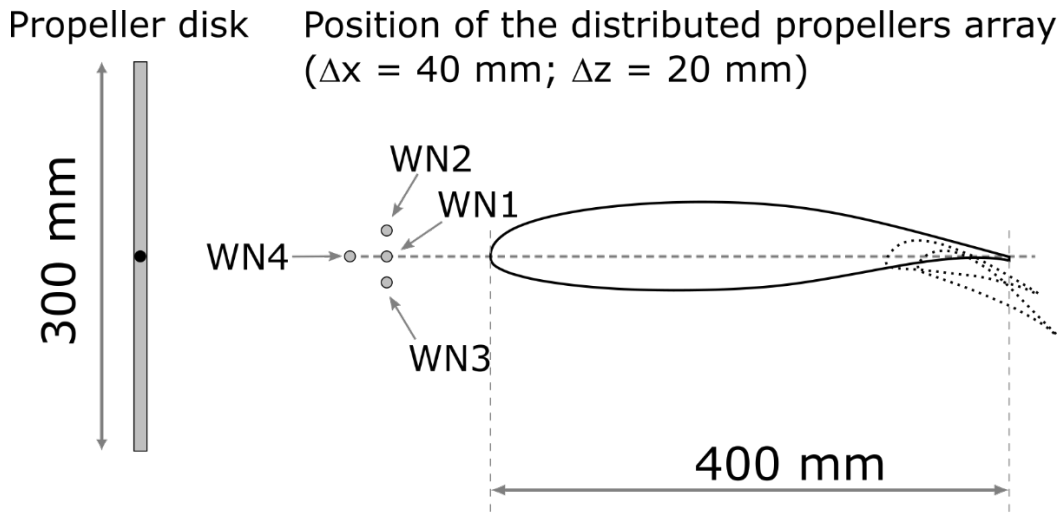

Figure 4.13 – DEP array positions

As the angle of attack α increases, initially the lift coefficient linearly increases. The trend of the drag coefficient C_D is well approximated by a parabola. At a certain angle of attack, the lift coefficient no longer increases and will tend to decrease, this phenomenon is called "stall". The maximum lift coefficient, $C_{L\max}$, corresponds to the stall. This does not imply that the wing is no longer load-bearing, but that it will only increase the drag coefficient. The stall phenomenon has been avoided in our test article.

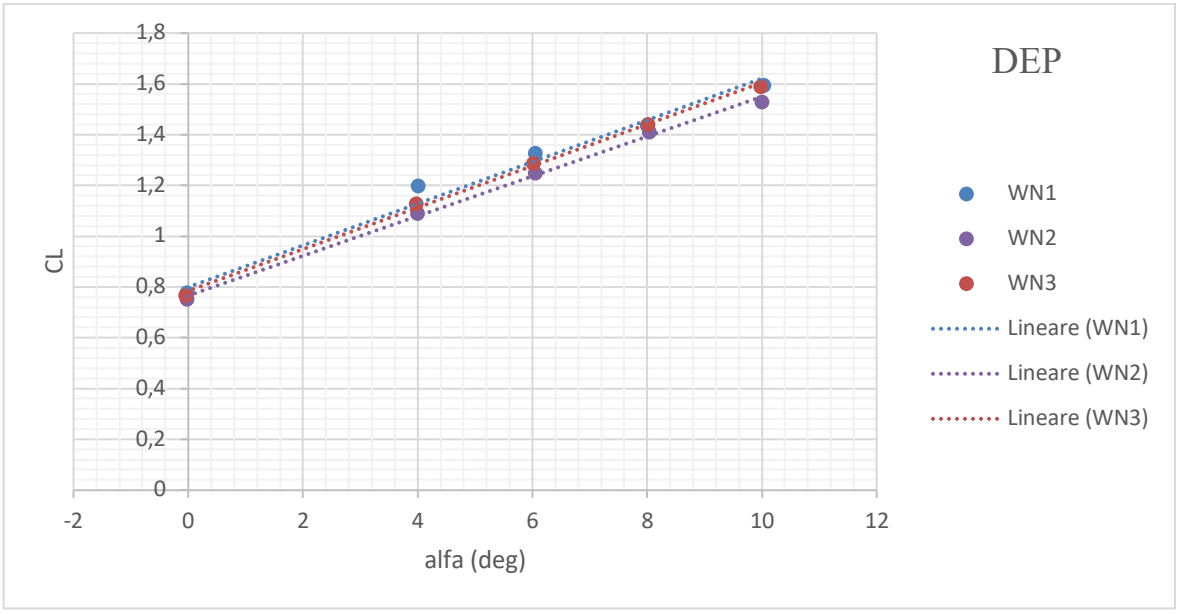

Figure 4.14 – C_L-α curve, flap 15°

Prop aligned wing chord plane is better for high lift, even if for very small values.

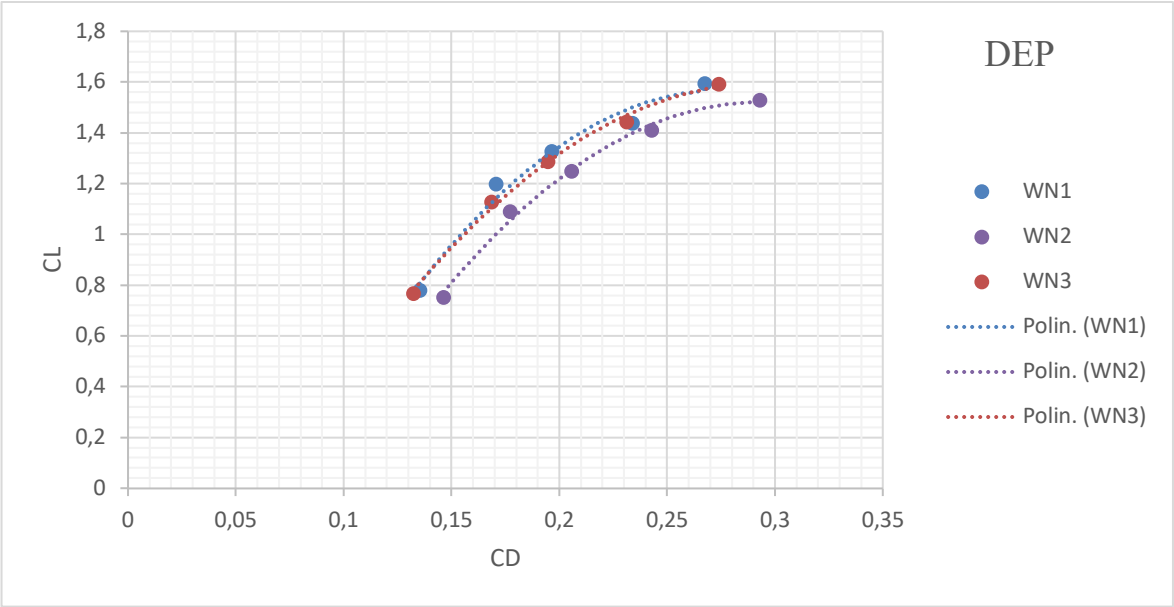

Figure 4.15 – $C_L - C_D$ polar curve, flap 15°

At lift coefficient values close to $C_{L\max}$, the efficiency at high trims increases. Aerodynamic efficiency is the ratio between lift L and drag D. Since we consider the airfoil, it also can be expressed as the ratio between the lift coefficient C_L and drag coefficient C_D. As previously stated, C_L and C_D depend on the same angle of attack and these two, in turn, are represented on a graph defined as the polar curve.

In **Figure 4.15**, it is shown the tendency of the $C_L - C_D$ curve. Also in this case, the propeller axis collinear with the wing chord plane (*WN1*) has a higher efficiency; even though it is not easy to distinguish from the trend of the propeller installed below the wing chord plane (*WN3*).

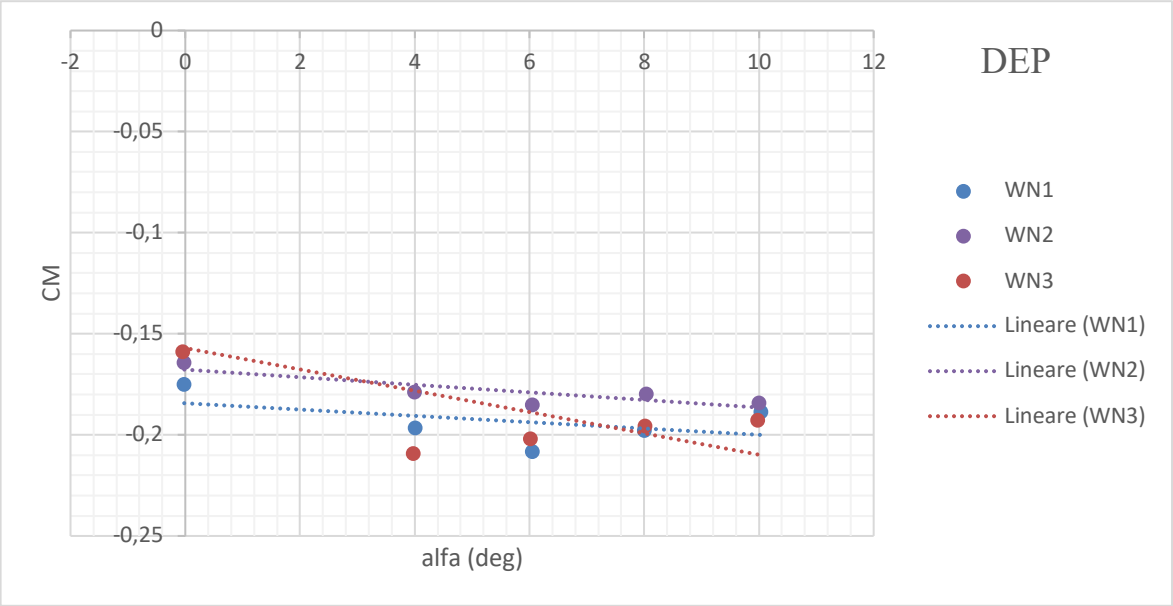

Figure 4.16 – $C_M - \alpha$ curve, static stability, flap 15°

Static stability occurs when, following a perturbation, the aircraft is subjected to a series of forces that bring it back to its initial condition. In other words, for static stability the pitching moment coefficient must be negative, so that in the case of positive vertical wind gust, the aircraft will tend to nose down to come back in the initial attitude.

The optimal moment coefficient is recorded for the propeller below the wing chord (*WN3*). The choice always falls on the C_M more negative than others, which corresponds to a higher efficiency and therefore higher values of the coefficient of lift. On the other side, this will be paid in terms of the horizontal tail's design.

Following, there are the same charts for the flap deflected at 30°.

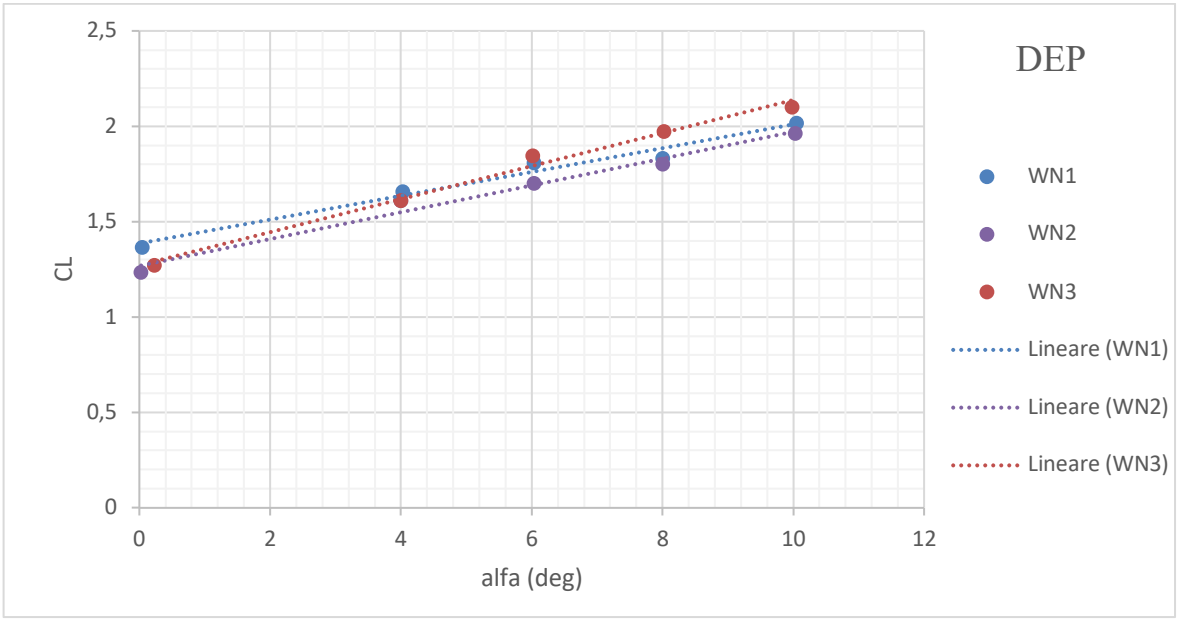

Figure 4.17 – C_L-α curve, flap 30°

Unlike the trend shown in **Figure 4.14**, the propeller below the wing chord's plane (*WN3*) is better for high lift; in fact, the gap between WN3 and WN1 is quite evident. Furthermore, with flaps deflected at 30°, the lift coefficient reaches the maximum value of 2.1. At 15 ° flap deflection, instead, a value of 1.6 is achieved.

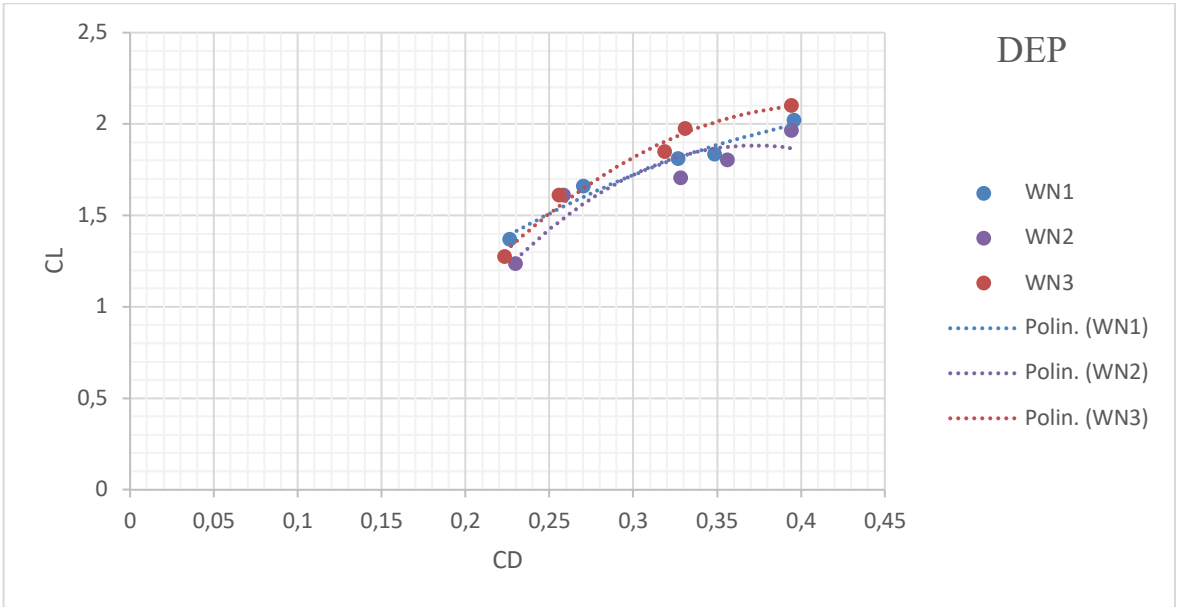

Figure 4.18 – $C_L - C_D$ polar curve, flap 30°

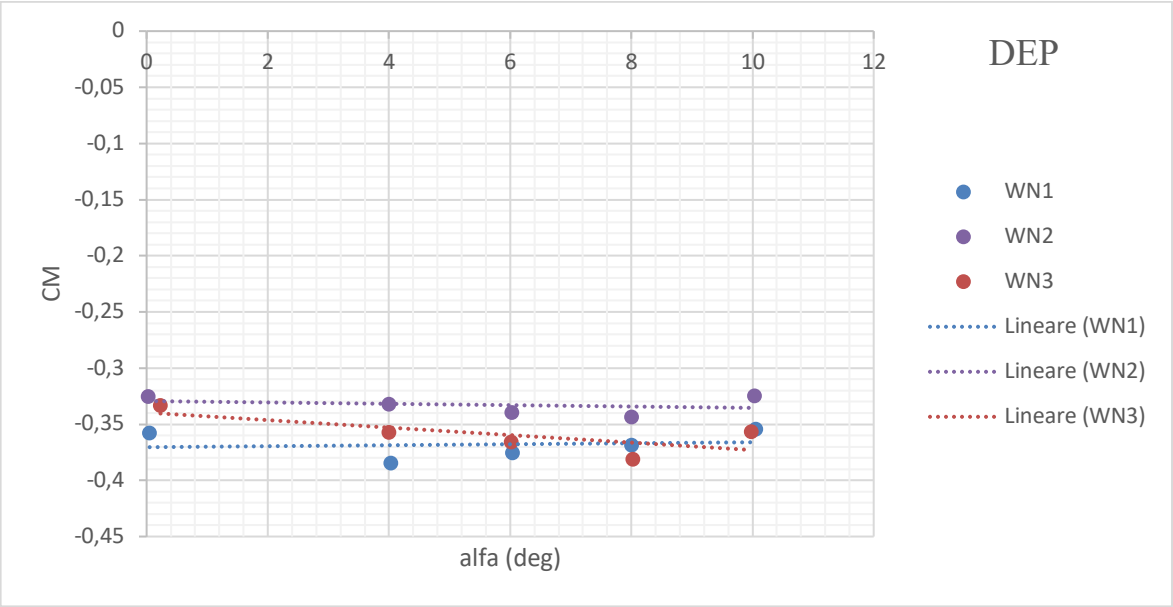

Figure 4.19 – $C_M - \alpha$ curve, static stability, flap 30°

Figures 4.18 and **4.19** show the trend of the polar curve and the moment coefficient. They differ from the previous graphs for the higher values, respectively around 2.2 and −0.3, with favorably results to the propeller below the wing's chord plane (*WN3*).

5. Conclusion

At the department of industrial engineering, in the main subsonic wind tunnel, a wing with flap, distributed propellers, and tip propeller has been installed. In the context of this thesis, the results for the tip propeller were not the scope of this thesis.

The model is a simple test case to investigate the aerodynamic forces and its coefficients, pressure measurements and propulsive forces. The main focus is on the position of distributed propellers array. Three different configurations were mounted: below, above and aligned with the plane of the wing chord.

The main advantages of our interest are:

- Aerodynamic efficiency L/D as high as possible.
- Negative values of the moment coefficient, in strict dependence on the values of the lift coefficient. As C_L increases, C_M will decrease.

Thus, in conclusion for what has been studied and recorded, test data highlight the benefits of installing the DEP array slightly below the wing chord's plane and as close as possible to the wing's leading edge to maximize the generation of high lift.

Bibliography

[1] V. Dezio, F. Nicolosi, D. Ciliberti, “Wind tunnel testing on the aerodynamics of the directional control surface of a generic regional transport airplane”, 2016-2017.

[2] Jewel B. Barlow William H. Rae, Jr. Alan Pope, "Low-Speed Wind Tunnel Testing", 3rd edition; February 1999.

[3] D. Ciliberti, F. Nicolosi, P. Della Vecchia, S. Corcione, V. Cusati, A. Alfano, P. Marsilia, B.S D’Abbusco, "Comparison of numerical and experimental analyses on a wing model with flap and distributed propulsion".

[4] Nicholas K. Borer, Michael D. Patterson, Jeffrey K. Viken, Mark D. Moore, JoeBen Bevirt, Alex M. Stoll and Andrew R. Gibson, "Design and Performance of the NASA SCEPTOR Distributed Electric Propulsion Flight Demonstrator", 2016.